Journal of Nuclear Materials 417 (2011) 93–98

Contents lists available at ScienceDirect

Journal of Nuclear Materials

journal homepage: www.elsevier.com/locate/jnucmat

Mechanical properties and TEM examination of RAFM steels irradiated up to 70 dpa in BOR-60

E. Gaganidze [a,*], C. Petersen [a], E. Materna-Morris [a], C. Dethloff [a], O.J. Weiß [a], J. Aktaa [a], A. Povstyanko [b], A. Fedoseev [b], O. Makarov [b], V. Prokhorov [b]

[a] Karlsruher Institut für Technologie, Institut für Angewandte Materialien, Hermann-von-Helmholtz-Platz 1, 76344 Eggenstein-Leopoldshafen, Germany
[b] Joint Stock Company "State Scientific Centre Research Institute of Atomic Reactors", 433510 Dimitrovgrad-10, Ulyanovsk Region, Russia[1]

ARTICLE INFO

Article history:
Available online 24 December 2010

ABSTRACT

Mechanical properties of Reduced Activation Ferritic/Martensitic (RAFM) steels were studied after irradiation in BOR-60 reactor to a neutron displacement damage of 70 dpa at 330–340 °C. Yield stress and Ductile-to-Brittle-Transition-Temperature of EUROFER97 indicate saturation of hardening and embrittlement. The phenomenological models for description of microstructure evolution and resulting irradiation hardening and embrittlement are discussed. The evolution of yield stress with dose is qualitatively understood within a Whapham and Makin model. Dislocation loops examined in TEM are considered a main source for low-temperature irradiation hardening. The analysis of the fatigue data in terms of the inelastic strain reveals comparable fatigue behaviour both for unirradiated and irradiated conditions, which can be described by a common Manson–Coffin relation. The study of helium effects in B-doped model steels indicated progressive material embrittlement with helium content. Post-irradiation annealing of RAFM steels yielded substantial recovery of mechanical properties.

1. Introduction

Structural materials for the in-vessel components of future energy generating Fusion Reactors (FR) will be exposed to high neutron and thermo-mechanical loads. Accumulated neutron displacement damage along with transmutation helium and hydrogen generated in the structure materials due to 14 MeV fusion neutrons strongly influences material embrittlement behaviour. The evolution of the microstructure, furthermore is very sensitive to the irradiation environment and temperature. Reduced Activation Ferritic/Martensitic (RAFM) steels are primary candidate structural materials for the First Wall (FW) and helium cooled Breeding Blanket (BB) with operating temperatures between 350 and 550 °C. Since a simulation facility with 14 MeV neutrons, like IFMIF, is not yet available, the irradiation performance of structural materials is often investigated in various Material Test Reactors. The neutron irradiation resistance of the European reference 9%Cr-WVTa steel EUROFER97 for the FW of the DEMO FR and other RAFM steels were thoroughly studied in various European irradiations up to neutron displacement damage doses of 70 dpa, see [1] and references therein. Although the radiation damage resistance of EUROFER97 and other 7–10%Cr-WVTa RAFM steels is superior to that of conventional Ferritic/Martensitic steels, the low temperature (<350 °C) irradiation hardening, accompanied by embrittlement and reduced ductility, remains the limiting factor for material application, indicating further needs of material development as well as new approaches in BB design optimisation. Furthermore, development of the modelling tools allowing the description of evolution of the microstructure and resulting irradiation hardening as well as transferability of the results to fusion relevant conditions is a mandatory step towards structural material qualification.

The present work focuses on the investigation and analysis of the mechanical properties of EUROFER97 and other RAFM steels irradiated in ARBOR 2 irradiation programme up to 70 dpa. The emphasis is on the evolution of the irradiation hardening and embrittlement with the irradiation dose. For the interpretation of the results, data from previous low and medium dose irradiations are also assessed [1]. The effects of helium are investigated in experimental boron doped heats. The neutron irradiation induced changes in the microstructure are examined by TEM (transmission electron microscopy). The role of the neutron irradiation induced defects in hardening and embrittlement is discussed. Modelling tools allowing the description of the irradiation induced microstructure evolution and related hardening are verified. The influence of the neutron irradiation on the low cycle fatigue (LCF) properties of RAFM steels is investigated.

* Corresponding author. Tel.: +49 7247 82 4083; fax: +49 7247 82 4566.
E-mail address: Ermile.Gaganidze@kit.edu (E. Gaganidze).
[1] adm@niiar.ru

0022-3115/$ - see front matter © 2010 Elsevier B.V. All rights reserved.
doi:10.1016/j.jnucmat.2010.12.047

Additional emphasis is put on the investigation of the effects of post-irradiation annealing on the mechanical properties of RAFM steels.

2. Experimental

2.1. Material

An industrial batch of the European RAFM steel EUROFER97 (nominal composition Fe–9Cr–1.1W–0.2V–0.12Ta, see e.g. [2]) was produced by Böhler Austria GmbH. Four different product forms: plates, with thicknesses of 8, 14, 25 mm and bars with diameter of 100 mm were distributed by KIT (formerly FZK) to different European associations. For the ARBOR irradiations some of the specimens (referred to as EUROFER97) were machined from 25 mm thick EUROFER97 plates in the as-delivered state (980 °C/0.5 h + 760 °C/1.5 h). Other specimens (referred to as EUROFER97 HT) were machined from 25 mm thick EUROFER97 plates subjected to a pre-irradiation heat treatment (1040 °C/0.5 h + 760 °C/1.5 h).

A 5-ton heat of modified F82H (F82H-mod, nominal composition Fe–7.5Cr–2W–0.15V–0.02Ta–0.1C) was produced by NKK Corporation for collaborative research coordinated by an International Energy Agency (IEA) committee. 7.5, 15 and 25 mm plates were distributed by IEA, and subsequently by KIT to the European partners. For the ARBOR irradiations the specimens were machined from 25 mm plate subjected to a heat treatment of 1040 °C/38 min + 750 °C/2 h.

Helium effects were investigated on EUROFER97 based experimental heats doped with different contents of natural boron and separated ^{10}B-isotope (0.008–0.112 wt.%) [3,4].

2.2. Irradiation experiment

The BOR-60 experimental fast reactor of JSC "SSC RIAR" offers different irradiation positions in the reactor core of 450 mm height and 550 mm diameter [5]. For the study of the high dose irradiation performance of EUROFER97 and other RAFM steels, 50% of the specimens from the ARBOR 1 irradiation [6] were reloaded into the ARBOR 2 rig for further irradiation to a target dose of 70 dpa at 330–340 °C. The irradiation rig instrumented with temperature and neutron monitors was loaded into the instrumented cell D-23 of BOR-60 allowing direct temperature measurement during the first campaign. The calculation of the damage dose for ferritic steel specimens was conducted using the SPECTER code [7]. A cumulative damage dose up to 70 dpa was achieved at 330–340 °C.

The ARBOR 2 irradiation included 144 mini-tensile/LCF specimens and 124 mini-impact (KLST) specimens of eleven different RAFM steels. KLST specimens were machined parallel to the rolling direction of the material plates (L–T orientation), see e.g. [2] for specimen geometry. Small size cylindrical specimens of 7.6 mm gauge length and 2 mm diameter were used for the investigation of tensile and LCF properties.

2.3. Post-irradiation examination

The post-irradiation mechanical testing of the specimens from the ARBOR 2 irradiation was performed at the material science laboratory of JSC "SSC RIAR" under ISTC Project 2781p.

Tensile and LCF tests were performed with an electro-mechanical testing machine equipped with a three-zone furnace and high-temperature extensometer [8]. Tensile specimens were tested under static (tensile) loading at different temperatures (250, 300 and 350 °C) with a strain rate of 3×10^{-3} s^{-1}. From the load–displacement curves, strength and ductility properties including the 0.2%-offset yield stress ($R_{p0.2}$), ultimate tensile strength (R_m), uniform strain (A_g) and fracture strain (A) were calculated. Reduction of area at fracture (Z) was measured from photos of the broken specimens taken after testing. The strain controlled push–pull (LCF) loading was performed at a constant temperature of 330 °C with different total strain ranges ($\Delta\varepsilon_{tot}$) between 0.8% and 1.2% and at common strain rate of 3×10^{-3} s^{-1}. The number of cycles to failure (N_f) was defined at a point where the peak tensile stress within a cycle decreased by 30% from its value at a point marking the termination of the linear dependence of peak tensile stress on the number of cycles (N). In addition, inelastic strain amplitudes ($\Delta\varepsilon_{inelastic}$) at $N_f/2$ were determined for given total strain amplitudes from the hysteresis loops.

Impact tests were performed with an instrumented impact testing facility [6]. The impact energies (E) vs. test temperature (T) curves were analyzed with respect to the upper shelf energy (*USE*) and the ductile-to-brittle transition temperature (*DBTT*), see e.g. [2] for the test and evaluation procedures.

Fractography of selected specimens were investigated by Scanning Electron Microscopy (SEM) in the hot cells of RIAR and in the Fusion Materials Laboratory of KIT. The microstructure was studied with TEM at KIT. TEM specimens were cut from the undeformed impact-specimens.

3. Results and discussion

3.1. Hardening and embrittlement

Fig. 1 presents the evolution of the hardening, as the increase in yield stress, with dose for EUROFER97 and F82H-mod for irradiation temperatures between 300 and 335 °C and for test temperatures between 300 and 350 °C. KIT results from ARBOR 2 as well as from the recent KIT irradiations programmes SPICE [3], WTZ 01/577 and ARBOR 1 [8] are presented by solid symbols. For comparison the literature results from [9–11] are also included in the diagram. Neutron irradiation leads to substantial increase in the yield stress with the dose. The yield stress increase is rather steep at doses below 10 dpa and in a good agreement with the observations on F82H after low-temperature irradiation [12]. In spite of large data scatter, partly due to different irradiation temperatures, a clear tendency to saturation at the achieved doses is identified for both RAFM steels.

Severe degradation of the tensile properties of RAFM steels observed in Fig. 1 is believed to be a result of neutron irradiation induced severe changes in the microstructure. Fig. 2 shows a weak

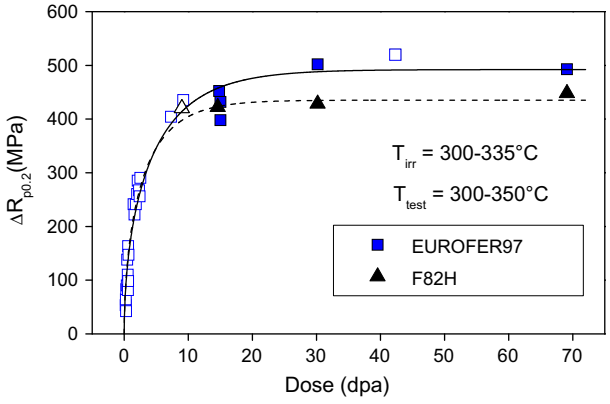

Fig. 1. Irradiation hardening vs. irradiation dose for EUROFER97 and F82H steels for T_{irr} = 300–335 °C and T_{test} = 300–350 °C. The full symbols represent KIT results. The open symbols are from the literature [9–11]. The solid line is a least square fit to the EUROFER97 data with Eq. (3). The dashed line is only a guide for eye.

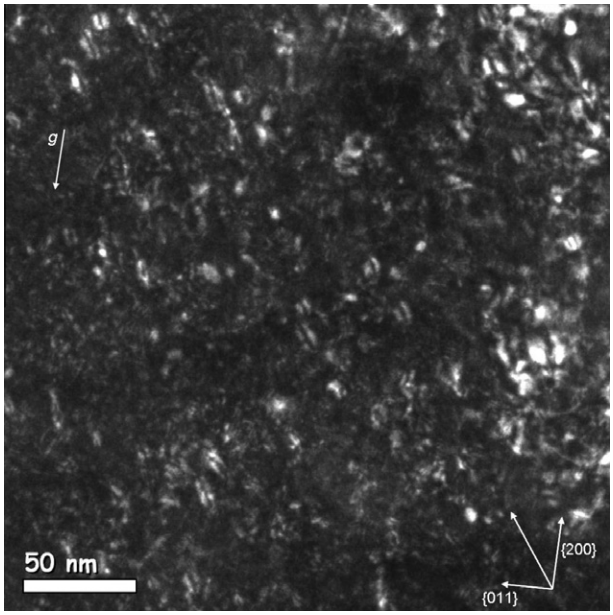

Fig. 2. TEM weak beam dark field image of EUROFER97 after irradiation in BOR-60 to ~32 dpa at 332 °C. Diffraction conditions: $g(4.1\,g)$ for $g = \{2\,0\,0\}$ near a $\langle 0\,1\,1\rangle$ zone axis.

beam dark field TEM micrograph of EUROFER97 after irradiation to a target dose of 32 dpa at 332 °C. The TEM sample was tilted to a $g(4.1\,g)$ diffraction condition using $g = \{2\,0\,0\}$ diffraction vector. Dislocation loops with diameters of up to 20 nm can be seen which appear edge on with a strong double arc contrast under this imaging condition. The evolution of the microstructure is very sensitive to the irradiation details, e.g. neutron flux and temperature. In contrast to the microstructure at $T_{irr} \geqslant 350$ °C, where most of the radiation defects are annealed, at $T_{irr} \leqslant 340$ °C formation of stable defects, e.g. vacancy and interstitial clusters and dislocation loops is observed. In addition to the displacement damage, irradiation enhanced diffusion leads to precipitation of brittle phases such as α'- and M_6C-phases. The formation of fine α'-precipitates was recently reported in [3]. Dislocation loops and α'-precipitates nearly homogeneously distributed in RAFM steels are believed to be a main source of the irradiation hardening and embrittlement.

The radiation defects acting as impeding obstacles to glide dislocations lead to strong material hardening which can be evaluated according to the following relationship

$$\Delta\sigma = M\alpha\mu b\sqrt{Nd} \tag{1}$$

with M being the Taylor factor, α – an average obstacle strength, μ – the shear modulus of the steel, b – the Burgers vector of the moving dislocation, N – the volume density of the obstacles and d – their average diameter. For the case when different obstacle types contribute to the hardening the resulting total hardening can be evaluated by $\Delta\sigma_{total} = \Sigma\Delta\sigma_i$, where the summation is done over all obstacle types i [13].

A phenomenological approach to the evolution of the radiation defect density with irradiation dose was given by Whapham and Makin in [14]. In this model the defect density N increases with dose at the initial stage of irradiation, but as their concentration increases the newly formed defects become captured by the already existing ones leading to a decrease of the number of newly formed defects during a given increment of dose as the dose increases. Hence, the increase in N and the achievement of a saturation value N_s is expected:

$$N = N_s\left[1 - \exp\left(-\frac{\Phi}{\Phi_0}\right)\right] \tag{2}$$

here Φ denotes the irradiation dose and Φ_0 is the scaling dose characterizing how fast the saturation of N sets in. For irradiation hardening dominated by a single obstacle type, combination of Eq. (2) with Eq. (1) yields the following relationship for the evolution of the irradiation hardening with dose:

$$\Delta\sigma = \Delta\sigma_s\sqrt{1 - \exp\left(-\frac{\Phi}{\Phi_0}\right)} \tag{3}$$

where $\Delta\sigma_s$ is the saturation value of hardening.

The solid line in Fig. 1 is a description of the irradiation hardening according to Eq. (3) with $\Delta\sigma_s = 492$ MPa and $\Phi_0 = 7.3$ dpa. In spite of: (i) differences in the irradiation conditions, e.g. the irradiation temperature, the neutron flux, (ii) differences in test conditions e.g. specimen geometry, strain rate and (iii) scatter of experimental data, Eq. (3) describes qualitatively the evolution of hardening with dose. Furthermore, the hardening rate appears to be significantly decreased at the achieved damage doses. Planned quantitative analysis of the radiation defects and their evolution with damage dose will shed more light on the hardening mechanisms.

Fig. 3 shows the impact energy vs. test temperature curves for EUROFER97, EUROFER97 HT and F82H-mod for the unirradiated condition, after neutron irradiation to 65–70 dpa at 335–337 °C and after post-irradiation heat treatment at 550 °C for 3 h. The neutron irradiation strongly degrades the impact properties leading to the shift of the *DBTT* towards higher temperatures and reduction of the USE. For the three irradiated materials, EUROFER97 HT exhibits the lowest *DBTT* after irradiation to 70 dpa/335 °C. F82H-mod irradiated to 65 dpa/337 °C behaves somewhat poorly compared to the EUROFER steels with respect to the both *DBTT* and USE. The post-irradiation annealing leads to strong recovery of the impact properties. The post-irradiation annealing of e.g. 70 dpa irradiated EUROFER97 HT at 550 °C for 3 h leads to a reduction of the *DBTT* from 135 to −43 °C resulting in a residual embrittlement (shift in *DBTT*) of just 48 °C compared to the unirradiated state. The residual embrittlement of F82H-mod irradiated to 65 dpa and annealed is about 106 °C.

Fig. 4 shows the evolution of the irradiation embrittlement (measured in impact tests) with dose for EUROFER97 and F82H steels at irradiation temperatures between 300 and 337 °C. For comparison the literature results from [11] are also included. In case of EUROFER97, differentiation is made between specimens machined from as-delivered products and specimens machined

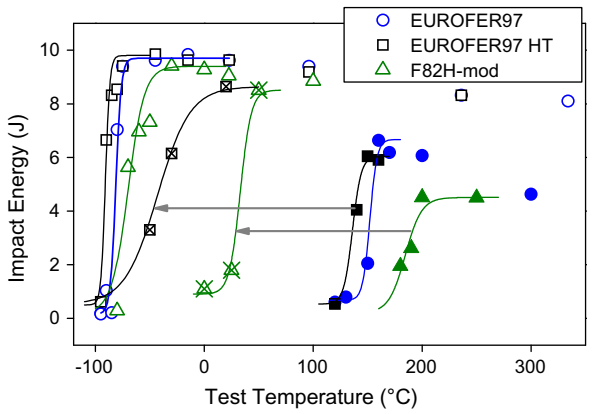

Fig. 3. Impact energy vs. test temperature for EUROFER97, EUROFER97 HT and F82H-mod in unirradiated (open symbols) condition, after irradiation in BOR-60 up to 65–70 dpa/335–337 °C (solid symbols) and after post-irradiation annealing at 550 °C for 3 h (crossed symbols). The lines are fits to the ductile-to-brittle-transition regions as described in [2]. The arrows indicate recovery of the impact properties after post-irradiation annealing.

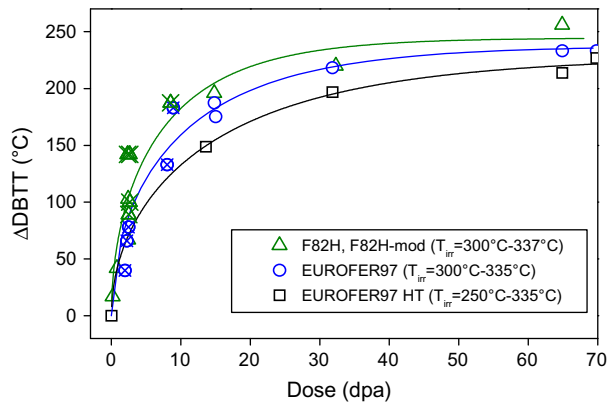

Fig. 4. Irradiation shifts of the *DBTT* vs. irradiation dose for EUROFER97, EUROFER97 HT and F82H steels. The open symbols represent KIT results and the crossed symbols are from [11]. The irradiation temperatures are indicated in the figure legend. The solid lines are a model description of the data, see text.

from the plates subjected to pre-irradiation heat treatment. The results on F82H and F82H-mod are plotted together for different heat treatments and material compositions [15]. These circumstances partly explain the large data scatter observed for F82H. The pre-irradiation heat treatment of EUROFER leads to considerable improvement of the irradiation resistance at doses up to 30 dpa. All three steels show steep increase in the $\Delta DBTT$ with dose below 10 dpa. This is in a good agreement with a strong embrittlement observed on F82H for different pre-irradiation heat treatment conditions after irradiation at 300 °C to 5 dpa [16]. At the achieved doses a clear tendency to saturation of embrittlement is identified. Indeed, for 70 dpa/335 °C irradiation the $\Delta DBTT$ of EUROFER97 is found to be 233 °C. This value is only 15 °C higher than the $\Delta DBTT$ after 32 dpa/332 °C irradiation.

The evolution of the irradiation embrittlement with dose in Fig. 4 is qualitatively similar to the evolution of the irradiation hardening in Fig. 1. This similarity allows the reasonable use of an equation similar to Eq. (3): $\Delta DBTT = \Delta DBTT_s\,(1 - \exp(-\Phi/\Phi_0))^{1/2}$, with $\Delta DBTT_s$ as the saturation embrittlement, for a phenomenological description of the dose dependence of the embrittlement. The solid lines in Fig. 4 are fit to the data with the above equation. A good qualitative description of the data is provided. The results for EUROFER97 are best described with $\Delta DBTT_s$ = 238 °C and Φ_0 = 16.7 dpa. Remarkably, for EUROFER97, Φ_0 determined for tensile hardening (in Fig. 1) is substantially less than Φ_0 determined for impact embrittlement (in Fig. 4), indicating that tensile hardening saturation is reached at lower levels of damage dose. This observation would suggest the existence of a non-hardening impact embrittlement mechanism in addition to hardening embrittlement, the former dominating at high damage doses.

Post-irradiation annealing leads to substantial improvement of the mechanical properties of RAFM steels in Fig. 3, indicating recovery of the radiation damage to a large extent. The recovery of the impact properties, however, seems to be sensitive to the prior radiation damage in these steels. The large residual embrittlement of F82H-mod in comparison with EUROFER97 indicates stronger degradation of the microstructure of F82H-mod under neutron irradiation. The pronounced growth of precipitates on block/packet and prior austenite grain boundaries in F82H after irradiation at 300 °C to 5 dpa [16] might be one of the possible reasons for large residual embrittlement, as the precipitates are expected to be stable under post-irradiation annealing. Formation of transmutation products is an additional source for the residual embrittlement. The investigation of the microstructure in post-irradiation annealed steels will provide more insight for the observed differences between EUROFER97 and F82H-mod steels. In contrast to the impact properties, the tensile properties show nearly complete recovery after post-irradiation annealing [1]. Having this in mind, the observed residual embrittlement in Fig. 3 might be an indication of the recovery of the hardening induced embrittlement only. The reproducibility of the mechanical properties recovery under repeatable irradiation and annealing conditions is one of the critical issues for validation of this method for application to the BB structures of a future FR.

3.2. Low cycle fatigue

Fig. 5 shows the number of cycles to failure (N_f) vs. inelastic strain range ($\Delta\varepsilon_{inelastic}$) for EUROFER97 and EUROFER97 HT steels in the unirradiated conditions and after neutron irradiation up to 70 dpa at 330–337 °C. The neutron irradiation seems to have little or no influence on the fatigue life in comparison to the unirradiated state for the adequate inelastic strains. Unfortunately, the limited number of available irradiated specimens does not allow detailed statistical analysis. Fig. 6 shows a SEM micrograph of the EUROFER97 HT specimen irradiated to 31 dpa/330 °C and LCF tested at

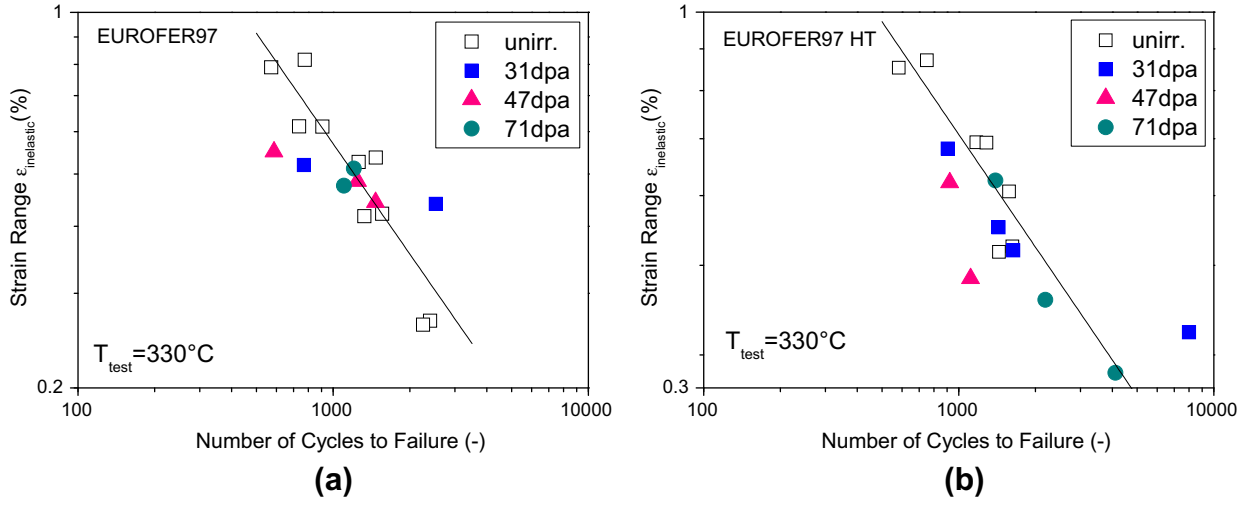

Fig. 5. Fatigue lifetime vs. inelastic strain range for unirradiated and irradiated (T_{irr} = 330–337 °C) EUROFER97 (a) and EUROFER97 HT (b). The lines represent the description of the unirradiated data by a Manson–Coffin relation.

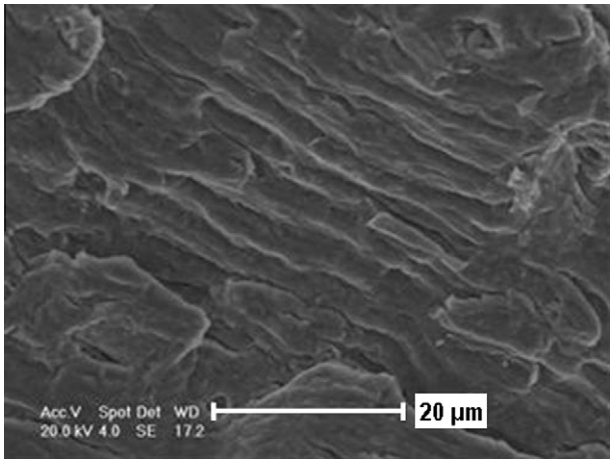

Fig. 6. SEM micrograph of the EUROFER97 HT specimen irradiated to 31 dpa in BOR-60 and LCF tested at 330 °C at $\Delta\varepsilon_{tot}$ = 1.2%.

330 °C with $\Delta\varepsilon_{tot}$ = 1.2% yielding N_f = 908. The fatigue fracture surface morphology reveals a terrace-like pattern indicating multiple deflections of the fatigue crack along its propagation path. Such crack deflections might be attributed to the interaction of the glide dislocations with obstacles, e.g. lath and prior austenite grain boundaries due to interruption of the slip bands at these obstacles.

In the low cycle fatigue regime the evolution of the fatigue life with inelastic strain can be described by the Manson–Coffin relationship

$$\Delta\varepsilon_{inelastic} = CN_f^m \quad (4)$$

with m and C as material and temperature dependent parameters. The lines in Fig. 5a and b represent the description of the unirradiated data with the above equation. The best fit were obtained with $m = -0.68$ and $m = -0.52$ for EUROFER97 and EUROFER97 HT, respectively. Most of the irradiated data is scattered around the unirradiated data in Fig. 5. Considering the large inherent scattering of fatigue life data this indicates little or no influence of the neutron irradiation on the fatigue damage behaviour. The apparent increase of the fatigue life observed in $\Delta\varepsilon_{tot}(N_f)$ representation in [8], is thus mainly related to the irradiation hardening observed in Fig. 1. Furthermore, a noticeable reduction of fatigue life for EUROFER97 for inelastic strain amplitudes above 0.5% in Fig. 5a can be recognized. The detailed analysis of the hysteresis loops of a specimen irradiated at 47 dpa and tested at $\Delta\varepsilon_{tot}$ = 1.1% ($\Delta\varepsilon_{inelastic}$ = 0.55% at $N_f/2$) indicated inelastic deformation even after the first quarter cycle. Under these circumstances, subsequent inelastic cyclic deformation is expected to occur within the grains in narrow slip bands which become cleaned of radiation defects, e.g. dislocation loops, by moving dislocations. As a result the deformation in these slip bands is enhanced and yields rapid strain softening. Thus, the reduction of the fatigue life in irradiated specimens at high strain amplitudes might be related to the micro crack initiation and the accumulation of fatigue damage in narrow slip bands. In addition, irradiation enhanced stresses compared to the unirradiated state for adequate inelastic strain might also accelerate the fatigue damage accumulation.

3.3. Helium effects

Fig. 7 shows the evolution of the helium induced extra embrittlement vs. helium content in model EUROFER97 based boron doped steels. The extra embrittlement is defined as *DBTT* shift in the boron doped heat after subtraction of the corresponding dpa induced *DBTT* shift in reference EUROFER97. Part of the results from SPICE and ARBOR 1 irradiations are reproduced from [4].

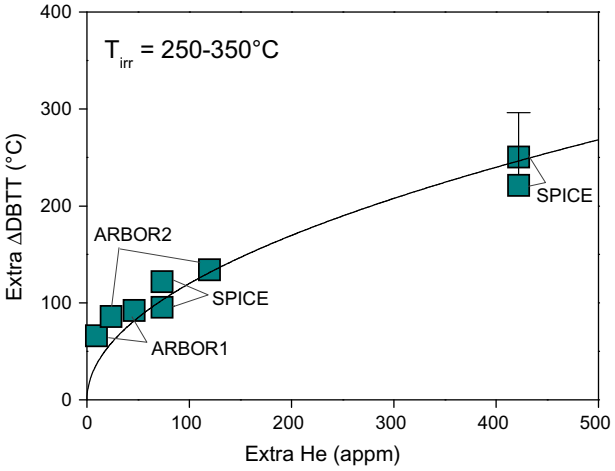

Fig. 7. Helium induced extra embrittlement vs. extra helium amount for irradiated boron doped steels. The line is a $A\sqrt{p_{He}}$ – type least square fit to the data, with A as fitting parameter.

The recent results from ARBOR 2 confirm the observed progressive embrittlement with increasing helium content for irradiation temperatures between 250 and 350 °C. The microstructure of the boron doped model alloy shown in Fig. 8 is characterised by helium bubbles rather homogeneously distributed in the steel matrix. Approximately 432 appm helium was produced by burn-up of 83 wppm ^{10}B-isotope under neutron irradiation [3,4].

The analysis of the hardening vs. embrittlement behaviour in SPICE experiment in [4] at $T_{irr} \leqslant 350$ °C and at helium contents up to 400 appm revealed helium induced embrittlement to be correlated to the hardening induced by helium bubbles. Under such circumstances, and taking into account a rather homogeneous distribution of the helium bubbles revealed in Fig. 8, the helium induced embrittlement is similar to Eq. (1) and can be phenomenologically described by a function of type $\Delta DBTT \propto (N_{He}d_{He})^{1/2} \propto (p_{He})^{1/2}$ (provided d_{He} = const.) [4]. The line in Fig. 7 represents the model description of the data with the above equation. Despite simplification of the model not taking into account e.g. different microstructure evolution in SPICE and ARBOR experiments due to different neutron spectra, possible non-uniform distribution of boron, e.g. preferentially on dislocations or prior austenite grain boundaries, the model describes the experimental data fairly well

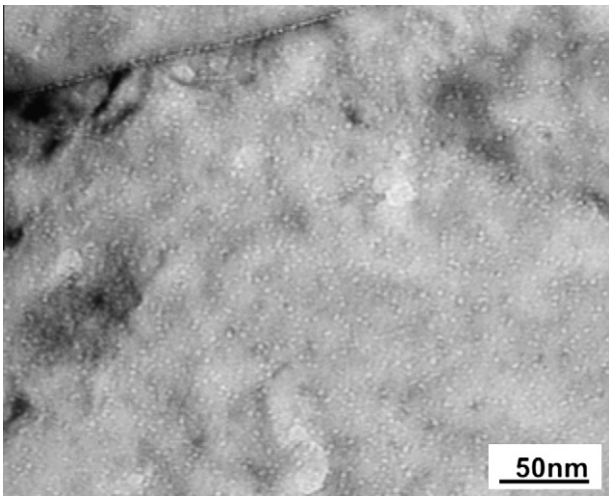

Fig. 8. TEM bright field image of the boron doped model alloy after irradiation in High Flux Reactor, Petten to ~15 dpa at 250 °C (~432 appm He).

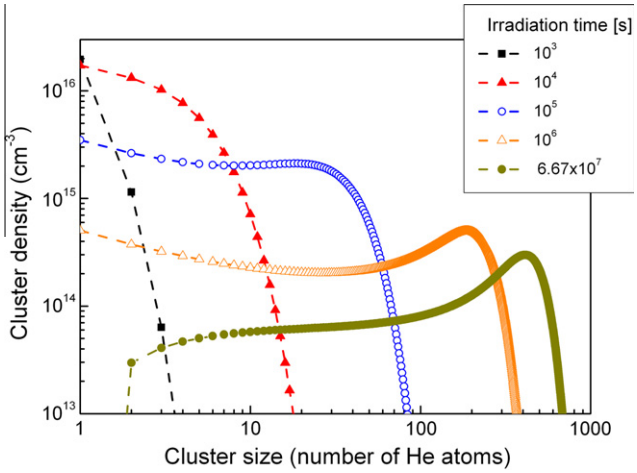

Fig. 9. Evolution of helium clusters with irradiation time at 250 °C in 83 wppm ^{10}B doped model alloy. Model calculation is done with dpa and helium production rates characteristic of the SPICE irradiation experiment.

for the investigated helium contents. Planned microstructural investigations for quantification of size, density and sites of helium bubbles in the boron doped heats will shed more light on the helium effects.

A phenomenological model was developed to describe helium cluster/bubble growth kinetics under irradiation. The evolution of the helium clusters with irradiation time is described using the Fokker–Plank approach to the rate theory for clustering [17]. The calculation of the cluster size dependent kinetic coefficients was performed with the helium diffusion coefficient as free parameter. Under assumption of homogeneous nucleation, the size distributions of helium clusters was obtained by numerical solution of the Fokker–Plank equation implemented in a FORTRAN code. Fig. 9 shows the evolution of the helium clusters at 250 °C in 83 wppm ^{10}B doped alloy with irradiation time up to the end of SPICE experiment (6.67×10^7 s). Model calculation is done with dpa and helium production rates characteristic for the SPICE experiment yielding a total amount of 432 appm helium after 10^7 s. A simulated final cluster size distribution obtained with a diffusivity of 4.32×10^{-12} cm^2/s is peaked at a cluster size of 410 helium atoms, corresponding to a bubble size of 2.1 nm which is in a good qualitative agreement with Fig. 8.

4. Conclusions

The influence of the neutron irradiation on the mechanical properties and microstructure of the RAFM steels was studied up to 70 dpa. The main conclusions of this study are summarized as follows:

1. Neutron irradiation leads to severe degradation of the mechanical properties at irradiation temperatures below $\leqslant$300–335 °C. Dislocation loops nearly homogeneously distributed in the steel matrix are believed to be the main source for the irradiation hardening and embrittlement.
2. Yield stress and *DBTT* of EUROFER97 indicate saturation of low temperature hardening and embrittlement at ~70 dpa. The evolution of the yield stress with dose is qualitatively understood with a Whapham and Makin model.
3. Neutron irradiation has only minor influence on the fatigue accumulation mechanism. The analysis of the data in terms of the inelastic strain reveals comparable fatigue behaviour for both unirradiated and irradiated conditions which can be described by a common Manson–Coffin relation.
4. Post-irradiation annealing of RAFM steels yields substantial recovery of the mechanical properties, indicating recovery of most of the radiation defects.
5. Helium production in boron doped steels leads to progressive material embrittlement with increasing helium content.

Acknowledgement

This work, supported by the European Communities under the contract of Association between EURATOM and Karlsruher Institut für Technologie, was carried out within the framework of the European Fusion Development Agreement. The views and opinions expressed herein do not necessarily reflect those of the European Commission.

This work is partly funded by Helmholtz Gemeinschaft e.V. under the Grant HRJRG-013.

References

[1] E. Gaganidze, H.-C. Schneider, C. Petersen, J. Aktaa, A. Povstyanko, V. Prokhorov, R. Lindau, E. Materna-Morris, A. Möslang, E. Diegele, R. Lässer, B. van der Schaaf, E. Lucon, in: Proc. of 22st IAEA Fusion Energy Conference, Geneva, Switzerland, 13–18 October 2008, Paper FT/P2-1.
[2] E. Gaganidze, H.-C. Schneider, B. Dafferner, J. Aktaa, J. Nucl. Mater. 355 (2006) 83–88.
[3] E. Materna-Morris, A. Möslang, R. Rolli, H.-C. Schneider, J. Nucl. Mater. 386–388 (2009) 422–425.
[4] E. Gaganidze, C. Petersen, J. Aktaa, J. Nucl. Mater. 386–388 (2009) 349–352; E. Gaganidze, J. Aktaa, Fusion Eng. Des. 83 (2008) 1498–1502.
[5] V.Sh. Sulaberidze et al., testing techniques, facilities and devices for irradiation test performance in the RIAR research reactors, Status and prospects for irradiation experiments in Russia/CIS, in: Proc. of 32. Japan Workshop, Oarai, Japan, 17 November 2004.
[6] C. Petersen, A. Povstyanko, V. Prokhorov, A. Fedoseev, O. Makarov, B. Dafferner, J. Nucl. Mater. 367–370 (2007) 544–549.
[7] L.R. Greenwood, R.K. Smither, SPECTER: Neutron Damage Calculations for Materials Irradiations, ANL/FPP/TM-197, 1985.
[8] C. Petersen, A. Povstyanko, V. Prokhorov, A. Fedoseev, O. Makarov, M. Walter, J. Nucl. Mater. 386–388 (2009) 299–302.
[9] A. Alamo, J.L. Bertin, V.K. Shamardin, P. Wident, J. Nucl. Mater. 367–370 (2007) 54–59.
[10] E. Lucon, Rachid Chaouadi, Marc Decreton, et al., J. Nucl. Mater. 329–333 (2004) 1078–1082.
[11] J. Rensman, NRG Irradiation Testing: Report on 300 °C and 60 °C Irradiated RAFM Steels, Petten 2005, 20023/05.68497/P.
[12] H. Tanigawa et al., J. Nucl. Mater. 386–388 (2009) 231–235.
[13] J. Aktaa, C. Petersen, J. Nucl. Mater. 389 (2009) 432–435.
[14] A.D. Whapham, M.J. Makin, Philos. Mag. 5 (51) (1960) 237–250.
[15] E. Gaganidze, Assessment of Impact Test Experiments on Irradiated EUROFER97 and other RAFM Steels, Forschungszentrum Karlsruhe, FZKA 7327, August 2007.
[16] H. Tanigawa et al., J. Nucl. Mater. 367–370 (2007) 42–47.
[17] S.V. Bulyarskii, V.V. Svetukhin, O.V. Prokhod'ko, Semiconductors 33 (1999) 1157–1162.